

Article

# Mode-Independent Optical Switch Based on Graphene-Polymer Hybrid Waveguides

Tianhang Lian, Yuhang Xie, Qidong Yu, Shijie Sun, Xiaoqiang Sun , Xibin Wang \*  and Daming Zhang 

State Key Laboratory of Integrated Optoelectronics, College of Electronic Science & Engineering, Jilin University, No. 2699 Qianjin Street, Changchun 130012, China; lianth18@mails.jlu.edu.cn (T.L.); xieyh22@mails.jlu.edu.cn (Y.X.); yuqd22@mails.jlu.edu.cn (Q.Y.); sjsun22@mails.jlu.edu.cn (S.S.); sunxq@jlu.edu.cn (X.S.); zhangdm@jlu.edu.cn (D.Z.)

\* Correspondence: xibinwang@jlu.edu.cn

**Abstract:** Mode-division multiplexing (MDM) is a promising multiplexing technique to further improve the transmission capacity of optical communication and on-chip optical interconnection systems. Furthermore, the multimode optical switch is of great importance in the MDM system, since it makes the MDM system more flexible by directly switching multiple spatial signals simultaneously. In this paper, we proposed a mode-independent optical switch based on the graphene–polymer hybrid waveguide platform that could process the TE<sub>11</sub>, TE<sub>12</sub>, TE<sub>21</sub> and TE<sub>22</sub> modes in a few-mode waveguide. The presented switch is independent of the four guided modes, optimizing the buried position of graphene capacitors in the polymer waveguide to regulate the coplanar interaction between the graphene capacitors and spatial modes. The TE<sub>11</sub>, TE<sub>12</sub>, TE<sub>21</sub> and TE<sub>22</sub> modes can be regulated simultaneously by changing the chemical potential of graphene capacitors in a straight waveguide. Our presented switch can enable the independent management of the spatial modes to be more flexible and efficient and has wide application in the MDM transmission systems.

**Keywords:** graphene; optical switch; polymer waveguide; mode-independent



**Citation:** Lian, T.; Xie, Y.; Yu, Q.; Sun, S.; Sun, X.; Wang, X.; Zhang, D.

Mode-Independent Optical Switch Based on Graphene-Polymer Hybrid Waveguides. *Photonics* **2023**, *10*, 1372. <https://doi.org/10.3390/photonics10121372>

Received: 3 November 2023

Revised: 7 December 2023

Accepted: 11 December 2023

Published: 13 December 2023



**Copyright:** © 2023 by the authors. Licensee MDPI, Basel, Switzerland. This article is an open access article distributed under the terms and conditions of the Creative Commons Attribution (CC BY) license (<https://creativecommons.org/licenses/by/4.0/>).

## 1. Introduction

Mode-division multiplexing (MDM) offers an advanced multiplexing technique to improve the transmission capacity of optical communication and on-chip optical interconnection systems by multiplexing different spatial modes within a few-mode fiber or waveguide [1–3]. Furthermore, the MDM system can be combined with the wavelength-division multiplexing technique to allow for an ultra-high data transmission rate in a single multimode waveguide [3]. Several key components required for realizing the MDM system have been developed, such as a mode (de)multiplexer [4], multimode crossing [5], multimode 3 dB splitter [6], higher-order mode filter [7], and multimode optical switch [8–10]. Among them, the multimode optical switch plays an important role in MDM systems, as it can switch the multiple spatial signals simultaneously and make the MDM system more flexible. For instance, a  $2 \times 2$  multimode optical switch based on a demultiplexing–processing–multiplexing technique has been reported for photonic networks-on-chip, resulting in a large footprint and complex on-chip management [9]. In recent years, research has been conducted to overcome this limitation [10]. At present, many reported MDM devices are mode-dependent or mode-independent for two or three spatial modes, and cannot take full advantage of the MDM system [11–13]. For the MDM system, the transmission capacity and efficiency will be improved by increasing the spatial modes that a single component can transmit and switch. Therefore, it is still highly desirable to design a mode-independent switch that supports more spatial modes to realize the mode-independent processing.

At present, optical switches have been developed based on different material platforms, such as silicon-on-insulator, silica and a polymer platform [14–17]. Graphene combined

with a polymer waveguide has provided a new platform for optical interconnection applications and attracted great attention in recent years [18–23]. Due to its excellent optical and electrical properties, graphene is a potential competitive candidate for the development of optoelectronic devices, such as optical modulators [15], optical switches [24–26], and phase array antenna [27]. The integration of graphene with polymer waveguide simplifies the fabrication processes to bury the graphene layer anywhere inside the waveguide. Meanwhile, the spatial modes in the waveguide can strongly interact with the graphene layers through the in-plane evanescent-field coupling. This new platform provides an approach to developing high-switching-efficiency, high-bandwidth, low-insertion loss-integrated switches with a small footprint that meet the requirements of complex structures and functions. In addition, in our previous work, we studied the application of graphene–polymer hybrid waveguides for the optical switch and modulator in optical communication systems [24,28–30].

In this paper, we proposed a mode-independent switch based on graphene–polymer hybrid waveguides, which can regulate the four spatial modes by sharing two graphene capacitors in the polymer waveguide. By applying the driving voltages to the graphene capacitors through graphene nanoribbons, the optical loss of  $TE_{11}$ ,  $TE_{12}$ ,  $TE_{21}$  and  $TE_{22}$  modes can be regulated with no significant difference. We designed a graphene capacitor and optimized the buried position to enable an almost identical switching efficiency for four spatial modes. The buried graphene capacitors inside the polymer waveguide core can improve the interaction between graphene and the optical field, which is helpful to reduce the power consumed by the device. Compared with the conventional multimode switch, our designed device can simplify the fabrication processes and regulate the guided spatial modes using a single component, which can reduce the footprint of the switch. Moreover, our presented device can process the guided modes directly, without using mode converters or other components, which is expected to improve the transmission capacity and switching efficiency of the MDM system.

## 2. Device Structure

A 3D schematic diagram of the proposed mode-independent switch is shown in Figure 1a. The presented device is based on a strip graphene–polymer hybrid waveguide on the silicon substrate. Figure 1b shows a cross-sectional view of the graphene–polymer hybrid waveguides, which are composed of a polymer few-mode waveguide and two graphene capacitors that share the same graphene ground electrode. In order to enable the waveguide to support  $TE_{11}$ ,  $TE_{12}$ ,  $TE_{21}$  and  $TE_{22}$  modes simultaneously, the width of the strip few-mode waveguide ( $w_{\text{core}}$ ) was designed to be 10  $\mu\text{m}$ . Meanwhile, the height of waveguide core ( $h_{\text{core}}$ ) was designed to be 0.5  $\mu\text{m}$  larger than  $w_{\text{core}}$  to avoid degenerate modes in the few-mode waveguide. The polymer material SU-8 2005 was employed as the waveguide core layer, which is technically convenient for burying the graphene capacitors. Then, the EpoClad cladding was fabricated on the chip via spin-coating method and protected the graphene nanoribbons of the connecting electrodes. For the few-mode waveguide, although the electric field distributions of the four spatial modes are different, they still have large overlapping regions. Therefore, each mode can be independently regulated by optimizing the buried position of the graphene capacitors. Both graphene capacitors have a sandwich structure, consisting of two single layers of graphene, and sharing the same lower graphene layer. The two graphene monolayers with a thickness of 0.35 nm are insulated by a 20 nm thick  $\text{Al}_2\text{O}_3$  film. The two graphene capacitors, buried in the same horizontal position inside the waveguide, are used to regulate the  $TE_{11}$ ,  $TE_{12}$ ,  $TE_{21}$  and  $TE_{22}$  modes by flexibly applying a drive voltage to Au electrodes. In this work, the refractive indices of the silicon, SU-8 2005, EpoClad and  $\text{Al}_2\text{O}_3$  were 3.450, 1.572, 1.559, and 1.732, respectively, under a 1550 nm wavelength.

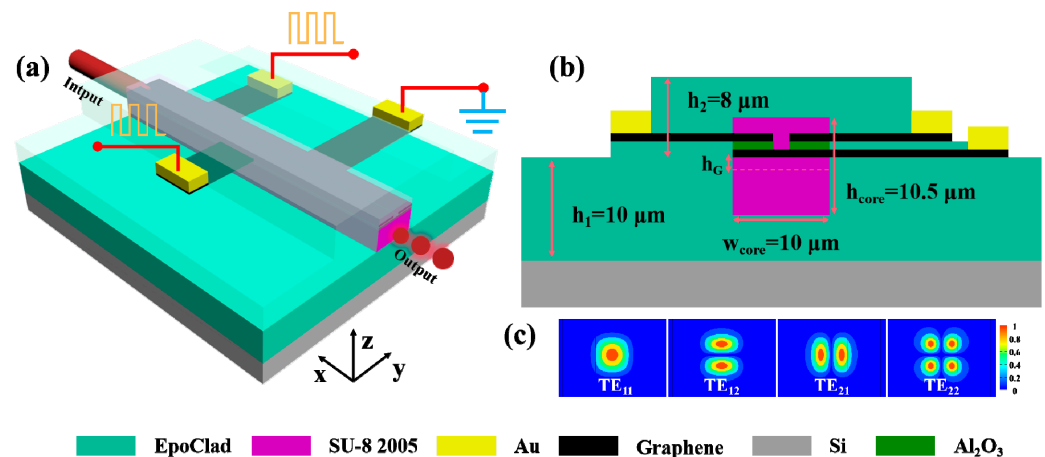


**Figure 1.** Illustration of the mode-independent optical switch configuration. (a) 3D view of the device. (b) Cross-sectional view of the waveguide. (c) The electric field distribution of TE<sub>11</sub>, TE<sub>12</sub>, TE<sub>21</sub> and TE<sub>22</sub> modes in the graphene–polymer hybrid waveguides.

Firstly, we optimized and simulated the structural parameters of the device based on the interface model of graphene with the commercial full-vector mode solver COMSOL [31]. In the simulation process, we only considered the mode power attenuation (MPA) induced by the graphene layers, while the losses caused by the absorption of polymer material and the coupling loss between the few-mode waveguide and fiber were not taken into account in the evaluation of the insertion losses and extinction ratio (ER). Figure 2a,b show the optimized results of the first designed device that buried one graphene capacitor in the waveguide. According to the electric field distribution of each mode, the graphene capacitor was buried in the middle of the waveguide, and then the influence of different locations on the MPA of each mode was analyzed. Figure 2a shows the simulated MPA of the TE<sub>11</sub>, TE<sub>12</sub>, TE<sub>21</sub> and TE<sub>22</sub> modes as a function of the buried position above the center position of the waveguide core. Significantly, the MPA of the four optical modes has nearly the same value above the center position of  $\sim 3 \mu\text{m}$ . This is ascribed to the similar strength in the interaction between graphene capacitor and each mode. In other words, the overlapping area between the graphene capacitor and each mode also affects the interaction strength. Therefore, we chose to bury the graphene capacitors  $2.9 \mu\text{m}$  above the center of the waveguide core to minimize the difference in the MPA of each mode, as shown in the inset of Figure 2a. Then, we simulated the MPA as a function of chemical potential, as shown in Figure 2b. According to the simulation results, the MPA has a consistent trend in different optical modes and shows no significant difference among them. The above study shows that the regulation effect of TE<sub>11</sub>, TE<sub>12</sub>, TE<sub>21</sub> and TE<sub>22</sub> modes is almost consistent when optimizing the position of the graphene capacitor. However, the MPA of the TE<sub>11</sub> and TE<sub>12</sub> modes is higher than that of the TE<sub>21</sub> and TE<sub>22</sub> modes. We next considered the second design that uses the structure of two graphene capacitors to further reduce the difference in MPA between different optical modes. Based on the electric field distribution of optical modes, we designed two graphene capacitors to share the same lower graphene electrode and increased the  $1.0 \mu\text{m}$  distance between them to reduce the graphene area. To study how the overlapping area between graphene capacitor and optical mode affects the MPA, we simulated the MPA of different modes with graphene capacitors at different positions, as shown in Figure 2c. It is clear that the difference in MPA between the four modes at around  $3 \mu\text{m}$  is significantly smaller than that of Figure 2a. This is due to the reduced graphene area, which did not impact the regulation effect of TE<sub>21</sub> and TE<sub>22</sub> modes while reducing the interaction intensity between the graphene capacitor and TE<sub>11</sub> or TE<sub>12</sub> modes. In other words, the electric field intensity of the TE<sub>21</sub> and TE<sub>22</sub> modes at the gap between the two graphene capacitors is very weak, while the TE<sub>12</sub> and TE<sub>11</sub> modes were in a zone with maximum electric field intensity. Hence, we chose to bury the graphene capacitors  $2.84 \mu\text{m}$  above the center of the waveguide core to minimize the MPA difference

between each mode, as shown in the inset of Figure 2c. Then, we simulated the MPA as a function of chemical potential, as shown in Figure 2d. The results in Figure 2d show an insignificant difference between the four modes of no more than 6 dB/cm, which is almost three times lower than that obtained in Figure 2b. The optimized device further reduces the MPA difference between different spatial modes and realizes the independent regulation of TE<sub>11</sub>, TE<sub>12</sub>, TE<sub>21</sub> and TE<sub>22</sub> modes. In addition, the MPA of the guided modes sharply decreases when the chemical potential is  $\mu > 0.1$  eV, and then remains at a low level, which shows that the waveguide exhibits a large absorption coefficient of optical signal when  $\mu = 0.1$  eV. Then, the optical signal can be transmitted through the waveguide with relatively low loss when  $\mu = 0.8$  eV. Hence, we chose the chemical potential  $\mu = 0.1$  eV and 0.8 eV as the “OFF” state and “ON” state of the device, respectively.

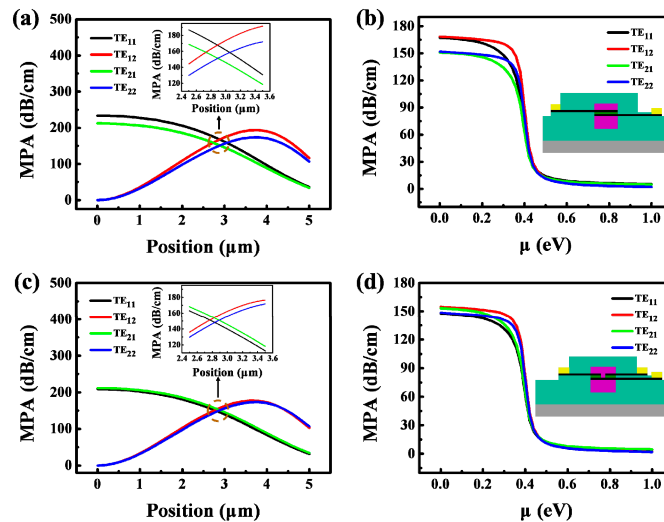


**Figure 2.** The mode-independent optical switch based on graphene–polymer hybrid waveguides with different designs for the graphene capacitor. First design scheme: (a) the MPA of different spatial modes varies with the graphene capacitors at different buried positions; (b) the MPA of different spatial modes varies with the chemical potential, and the inset shows a cross-sectional view of the graphene capacitor. Second design scheme: (c) the MPA of different spatial modes varies with the graphene capacitor at different buried positions; (d) the MPA of different spatial modes varies with the chemical potential, and the inset shows a cross-sectional view of the graphene capacitors.

Next, we further analyzed the transmission properties of the device. Figure 3 shows that the normalized transmission of the four guided modes varies with the graphene length under the “ON” and “OFF” states. The output power for each guided mode under the “ON” state is about 96% when the graphene length reaches 1000  $\mu\text{m}$ . In the “OFF” state, the output power for each guided mode is about 3%. The results show that the device can realize the ON-OFF control of the signal. In order to intuitively observe the transmission conditions of each guided mode under “ON” and “OFF” working states, the simulation was carried out in a three-dimensional (3D) environment. Figure 4 shows the 3D optical transmission of different optical modes operating under “ON” and “OFF” states when the graphene length is 1000  $\mu\text{m}$ . As shown in Figure 4a, the electric field intensity decreases with the increase in transmission distance when the device operates under the “OFF” state. Figure 4b shows that the electric field intensity remains stable as the transmission distance increases when the device operates under the “ON” state. The 3D optical transmission simulations indicate that the optical signal can be regulated by the electrical absorption characteristics of graphene capacitors.

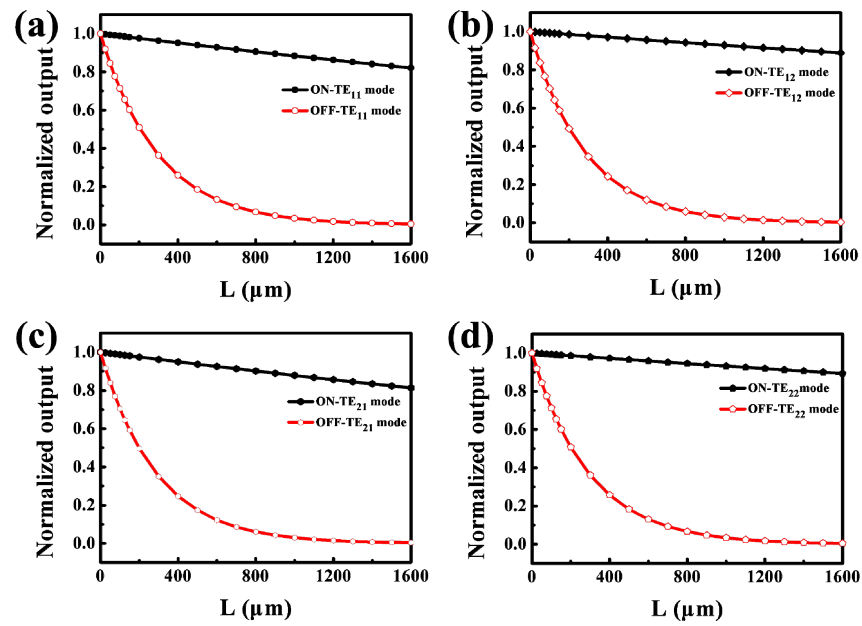


Figure 3. Normalized output power varies with the graphene length in “ON” and “OFF” states for (a) TE<sub>11</sub>, (b) TE<sub>12</sub>, (c) TE<sub>21</sub>, and (d) TE<sub>22</sub> modes.

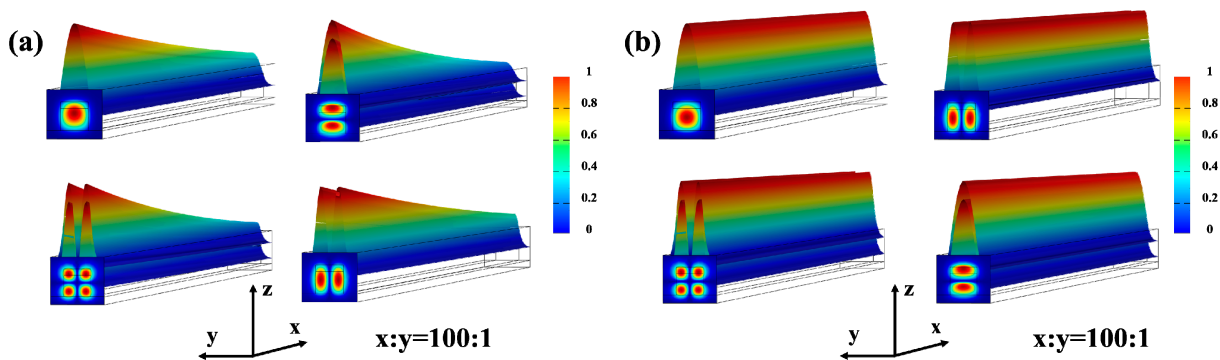
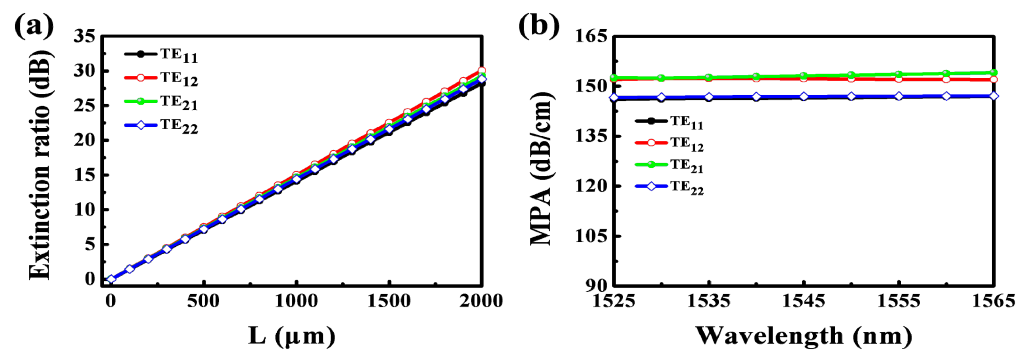


Figure 4. The propagation paths of of TE<sub>11</sub>, TE<sub>12</sub>, TE<sub>21</sub> and TE<sub>22</sub> modes in the graphene–polymer hybrid waveguides in the (a) “OFF” state and (b) “ON” state, respectively.

We further characterized the performance of the device after optimizing the structural parameters of the device. Figure 5a shows the relationship between the ER and graphene capacitor length for TE<sub>11</sub>, TE<sub>12</sub>, TE<sub>21</sub> and TE<sub>22</sub> modes. The ER for the guided modes remains consistent under the same length of graphene capacitor. When the transmission length is greater than 1500 μm, the ER of guided modes can exceed 20 dB. Then, we simulated the varied wavelength influence on MPA for TE<sub>11</sub>, TE<sub>12</sub>, TE<sub>21</sub> and TE<sub>22</sub> modes over the C-band when  $\mu = 0.1$  eV, as shown in Figure 5b. According to the simulation results, we can see that the MPA of guided modes is ~150 dB/cm and remains at a relatively stable level within the C-band, which shows that the presented device can operate stably in a broad band. Finally, we studied the dynamic response of the proposed device based on the equivalent electrical circuit model. The power consumption can be defined as  $E_{\text{bit}} = C(\Delta U)^2/4$ , where the switch voltage is 1.84 V. Then, the calculated power consumption for TE<sub>11</sub>, TE<sub>12</sub>, TE<sub>21</sub> and TE<sub>22</sub> modes is about 38.4 pJ/bit, and the corresponding switching times are about 115 ps for the guided modes.



**Figure 5.** (a) The extinction ratios of the mode-independent switch as a function of the graphene capacitor length for TE<sub>11</sub>, TE<sub>12</sub>, TE<sub>21</sub> and TE<sub>22</sub> modes. (b) The varied wavelength influence on MPA of TE<sub>11</sub>, TE<sub>12</sub>, TE<sub>21</sub> and TE<sub>22</sub> modes.

### 3. Conclusions

In summary, we presented a mode-independent switch operating in the C-band to simultaneously switch the TE<sub>11</sub>, TE<sub>12</sub>, TE<sub>21</sub> and TE<sub>22</sub> modes by utilizing the coplanar interaction between the buried graphene capacitors and spatial modes. The device was designed based on the graphene–polymer hybrid waveguide platform, which is helpful to bury the graphene capacitors inside the waveguide core. The two graphene capacitors share the same lower graphene electrode, and the distance between them is 1.0 μm. By varying the chemical potential of graphene capacitors, the TE<sub>11</sub>, TE<sub>12</sub>, TE<sub>21</sub> and TE<sub>22</sub> modes can be simultaneously regulated without differentiation. The ERs for the guided modes are around 23 dB, with a switching voltage of 1.84 V, when the effective length of the active region exceeds 1500 μm. The power consumption of the guided modes is ~38.4 pJ/bit. Compared with the traditional device based on an inorganic waveguide-integrated graphene [32], the proposed device is superior in terms of the number of supported modes and the switching voltage, which can improve the transmission capacity and switching efficiency. Meanwhile, the system complexity and power consumption can also be reduced by decreasing the external, individual, arranged channels. The designed device, with the function of mode-independent regulation, can be applied in high-density integrated optoelectronic device to improve the transmission capacity, which is extremely promising for applications in the MDM system. Moreover, by designing different waveguide structures and combining the advantages of the flexible polymer waveguide fabrication process, the present structure can also be extended to other devices, such as optical attenuators, optical modulators, and photodetectors.

**Author Contributions:** Methodology, software, validation, writing—original draft, T.L.; software, resources, writing—review and editing, Y.X.; investigation, Q.Y.; software, resources, S.S.; funding acquisition, writing—review and editing, X.S.; conceptualization, writing—review and editing, funding acquisition, X.W.; formal analysis, writing—review and editing, D.Z. All authors have read and agreed to the published version of the manuscript.

**Funding:** This work was supported by the National Key R&D Program of China (2021YFB2800202); Jilin Province Development and Reform Commission Project (No. 2023C030-7); National Natural Science Foundation of China (61875069).

**Institutional Review Board Statement:** Not applicable.

**Informed Consent Statement:** Not applicable.

**Data Availability Statement:** Data are contained within the article.

**Conflicts of Interest:** The authors declare no conflict of interest.

## References

1. Hanzawa, N.; Saitoh, K.; Sakamoto, T.; Matsui, T.; Tsujikawa, K.; Koshiba, M.; Yamamoto, F. Mode multi/demultiplexing with parallel waveguide for mode division multiplexed transmission. *Opt. Express* **2014**, *22*, 29321–29330. [[CrossRef](#)]
2. Wang, J.; Chen, P.X.; Chen, S.T.; Shi, Y.C.; Dai, D.X. Improved 8-channel silicon mode demultiplexer with grating polarizers. *Opt. Express* **2014**, *22*, 12799–12807. [[CrossRef](#)]
3. Luo, L.W.; Ophir, N.; Chen, C.P.; Gabrielli, L.H.; Poitras, C.B.; Bergmen, K.; Lipson, M. WDM-compatible mode-division multiplexing on a silicon chip. *Nat. Commun.* **2014**, *5*, 3069. [[CrossRef](#)] [[PubMed](#)]
4. Ding, Y.H.; Xu, J.; Da Ros, F.; Huang, B.; Ou, H.Y.; Peucheret, C. On-chip two-mode division multiplexing using tapered directional coupler-based mode multiplexer and demultiplexer. *Opt. Express* **2013**, *21*, 10376–10382. [[CrossRef](#)] [[PubMed](#)]
5. Xu, H.N.; Shi, Y.C. Metamaterial-based maxwell's fisheye lens for multimode waveguide crossing. *Laser Photonics Rev.* **2018**, *12*, 1800094. [[CrossRef](#)]
6. Luo, Y.C.; Yu, Y.; Ye, M.Y.; Sun, C.L.; Zhang, X.L. Integrated dual-mode 3dB power coupler based on tapered directional coupler. *Sci. Rep.* **2016**, *6*, 23516. [[CrossRef](#)] [[PubMed](#)]
7. Guan, X.W.; Ding, Y.H.; Frandsen, L.H. Ultra-compact broadband higher order-mode pass filter fabricated in a silicon waveguide for multimode photonics. *Opt. Lett.* **2015**, *40*, 3893–3896. [[CrossRef](#)] [[PubMed](#)]
8. Chen, K.X.; Yan, J.L.; He, S.L.; Liu, L. Broadband optical switch for multiple spatial modes based on a silicon densely packed waveguide array. *Opt. Lett.* **2019**, *44*, 907–910. [[CrossRef](#)]
9. Jia, H.; Zhou, T.; Zhang, L.; Ding, J.F.; Fu, X.; Yang, L. Optical switch compatible with wavelength division multiplexing and mode division multiplexing for photonic networks-on-chip. *Opt. Express* **2017**, *25*, 20698–20707. [[CrossRef](#)]
10. Xiong, Y.L.; Priti, R.B.; Liboiron-Ladouceur, O. High-speed two-mode switch for mode-division multiplexing optical networks. *Optica* **2017**, *4*, 1098–1102. [[CrossRef](#)]
11. Zhang, Y.; Zhang, R.H.; Zhu, Q.M.; Yuan, Y.; Su, Y.K. Architecture and devices for silicon photonic switching in wavelength, polarization and mode. *J. Lightw. Technol.* **2020**, *38*, 215–225. [[CrossRef](#)]
12. Yang, L.; Zhou, T.; Jia, H.; Yang, S.L.; Ding, J.F.; Fu, X.; Zhang, L. General architectures for on-chip optical space and mode switching. *Optica* **2018**, *5*, 180–187. [[CrossRef](#)]
13. Stern, B.; Zhu, X.L.; Chen, C.P.; Tzuang, L.D.; Cardenas, J.; Bergman, K.; Lipson, M. On-chip mode-division multiplexing switch. *Optica* **2015**, *2*, 530–535. [[CrossRef](#)]
14. Kumar, S.; Raghuvanshi, S.K.; Kumar, A. Implementation of optical switches using Mach-Zehnder interferometer. *Opt. Eng.* **2013**, *52*, 097106. [[CrossRef](#)]
15. Brunetti, G.; Marocco, G.; Di Benedetto, A.; Giorgio, A.; Armenise, M.N.; Ciminelli, C. Design of a large bandwidth  $2 \times 2$  interferometric switching cell based on a sub-wavelength grating. *J. Opt.* **2021**, *23*, 085801. [[CrossRef](#)]
16. DasMahapatra, P.; Stabile, R.; Rohit, A.; Williams, K.A. Optical crosspoint matrix using broadband resonant switches. *IEEE J. Sel. Top. Quant.* **2014**, *20*, 5900410. [[CrossRef](#)]
17. Lin, B.Z.; Sun, S.J.; Sun, X.Q.; Lian, T.H.; Zhu, M.; Che, Y.H.; Wang, X.B.; Zhang, D.M. Dual-mode  $2 \times 2$  thermo-optic switch based on polymer waveguide Mach-Zehnder interferometer. *IEEE Photonics Technol. Lett.* **2022**, *34*, 1317–1320. [[CrossRef](#)]
18. Sun, Z.P.; Popa, D.; Hasan, T.; Torrisi, F.; Wang, F.Q.; EKelleher, E.J.R.; Travers, J.C.; Nicolosi, V.; Ferrari, A.C. A stable, wideband tunable, near transform-limited, graphene-mode-locked, ultrafast laser. *Nano Res.* **2010**, *3*, 653–660. [[CrossRef](#)]
19. Ye, S.W.; Wang, Z.S.; Tang, L.F.; Zhang, Y.L.; Lu, R.G.; Liu, Y. Electro-absorption optical modulator using dual-graphene-on-graphene configuration. *Opt. Express* **2014**, *22*, 26173–26180. [[CrossRef](#)]
20. Kim, J.T.; Choi, C.G. Graphene-based polymer waveguide polarizer. *Opt. Express* **2012**, *20*, 3556–3562. [[CrossRef](#)]
21. Guo, J.S.; Li, J.; Liu, C.Y.; Yin, Y.L.; Wang, W.H.; Ni, Z.H.; Fu, Z.L.; Yu, H.; Xu, Y.; Shi, Y.C.; et al. High-performance silicon-graphene hybrid plasmonic waveguide photodetectors beyond 1.55  $\mu\text{m}$ . *Light Sci. Appl.* **2020**, *9*, 29. [[CrossRef](#)] [[PubMed](#)]
22. Chen, W.C.; Guo, R.X.; Wan, D.; Sharma, T.; Zhang, L.; Liu, T.G.; Cheng, Z.Z. Design of a graphene-enabled dual-mode kerr frequency comb. *IEEE J. Sel. Top. Quantum Electron.* **2022**, *28*, 5100107. [[CrossRef](#)]
23. Xing, Z.K.; Li, C.; Han, Y.D.; Hu, H.F.; Cheng, Z.Z.; Wang, J.Q.; Liu, T.G. Waveguide-integrated graphene spatial mode filters for on-chip mode-division multiplexing. *Opt. Express* **2019**, *27*, 19188–19195. [[CrossRef](#)] [[PubMed](#)]
24. Wang, X.B.; Jin, W.; Chang, Z.S.; Kin, S.C. Buried graphene electrode heater for a polymer waveguide thermo-optic device. *Opt. Lett.* **2019**, *44*, 1480–1483. [[CrossRef](#)] [[PubMed](#)]
25. Jiang, L.Z.; Huang, Q.D.; Kin, S.C. Low-power all-optical switch based on a graphene-buried polymer waveguide Mach-Zehnder interferometer. *Opt. Express* **2022**, *30*, 6786–6797. [[CrossRef](#)] [[PubMed](#)]
26. Tavana, S.; Bahadori-Haghighi, S.; Sheikhi, M.H. High-performance electro-optical switch using an anisotropic graphene-based one-dimensional photonic crystal. *Opt. Express* **2022**, *30*, 9269–9283. [[CrossRef](#)]
27. Wang, Y.; Wang, Y.; Li, Q.Y.; Zhang, Y.; Yan, S.Y.; Wang, C.H. Tunable graphene-based metasurface for an ultra-low sidelobe terahertz phased array antenna. *Opt. Express* **2021**, *29*, 26865–26875. [[CrossRef](#)]
28. Lian, T.H.; Yang, K.D.; Wang, X.B.; Jiang, M.H.; Sun, S.J.; Niu, D.H.; Zhang, D.M. Electro-absorption optical modulator based on graphene-buried polymer waveguides. *IEEE Photonics J.* **2022**, *12*, 6601610. [[CrossRef](#)]
29. Lian, T.H.; Yang, K.D.; Sun, S.J.; Zhu, M.; Yue, J.; Lin, B.Z.; Sun, X.Q.; Wang, X.B.; Zhang, D.M. Polarization-independent electro-absorption optical modulator based on trapezoid polymer-graphene waveguide. *Opt. Laser Technol.* **2022**, *149*, 107815. [[CrossRef](#)]

30. Lian, T.H.; Zhu, M.; Sun, S.J.; Sun, X.Q.; Che, Y.H.; Lin, B.Z.; Wang, X.B.; Zhang, D.M. Mode-selective modulator and switch based on graphene-polymer hybrid waveguides. *Opt. Express* **2022**, *30*, 23746–23755. [[CrossRef](#)]
31. Chang, Z.S.; Ching, K.S. Ultra-broadband mode filters based on graphene-embedded waveguides. *Opt. Lett.* **2017**, *42*, 3868–3871. [[CrossRef](#)] [[PubMed](#)]
32. Wang, J.Q.; Zhang, X.Y.; Chen, Y.Z.; Geng, Y.F.; Du, Y.; Li, X.J. Design of a graphene-based silicon nitride multimode waveguide-integrated electro-optic modulator. *Opt. Commun.* **2021**, *481*, 126531. [[CrossRef](#)]

**Disclaimer/Publisher’s Note:** The statements, opinions and data contained in all publications are solely those of the individual author(s) and contributor(s) and not of MDPI and/or the editor(s). MDPI and/or the editor(s) disclaim responsibility for any injury to people or property resulting from any ideas, methods, instructions or products referred to in the content.